IMA Journal of Applied Mathematics (2009) **74**, 230–249
doi:10.1093/imamat/hxn036
Advance Access publication on December 15, 2008

On the temporal stability of steady-state quasi-1D bubbly cavitating nozzle flow solutions

ŞENAY PASINLIOĞLU†
Faculty of Science and Letters, Department of Mathematics, Istanbul Technical University, 34469 Maslak, Istanbul, Turkey

CAN F. DELALE‡
Faculty of Aeronautics and Astronautics, Istanbul Technical University, 34469 Maslak, Istanbul, Turkey and TÜBİTAK Feza Gürsey Institute, PO Box 6, 81220 Çengelköy, Istanbul, Turkey

AND

GÜNTER H. SCHNERR§
Lehrstuhl für Fluidmechanik—Fachgebiet Gasdynamik, Technische Universität München Boltzmannstrasse 15, D-85747 Garching, Germany

[Received on 15 October 2007; revised on 26 June 2008; accepted on 23 October 2008]

Quasi-1D unsteady bubbly cavitating nozzle flows are considered by employing a homogeneous bubbly liquid flow model, where the non-linear dynamics of cavitating bubbles is described by a modified Rayleigh–Plesset equation. The various damping mechanisms are considered by a single damping coefficient lumping them together in the form of viscous dissipation and by assuming a polytropic law for the expansion and compression of the gas. The complete system of equations, by appropriate uncoupling, are then reduced to two evolution equations, one for the flow speed and the other for the bubble radius when all damping mechanisms are considered by a single damping coefficient. The evolution equations for the bubble radius and flow speed are then perturbed with respect to flow unsteadiness resulting in a coupled system of linear partial differential equations (PDEs) for the radius and flow speed perturbations. This system of coupled linear PDEs is then cast into an eigenvalue problem and the exact solution of the eigenvalue problem is found by normal mode analysis in the inlet region of the nozzle. Results show that the steady-state cavitating nozzle flow solutions are stable only for perturbations with very small wave numbers. The stable regions of the stability diagram for the inlet region of the nozzle are seen to be broadened by the effect of turbulent wall shear stress.

Keywords: bubbly cavitating flows; steady-state solutions; temporal stability.

1. Introduction

Cavitating flows through converging–diverging nozzles seem to be the simplest configurations for analysis in hydrodynamic cavitation. They have direct applications in cavitation in ducts and venturi tubes as

†Email: pasinliogl@itu.edu.tr
‡Corresponding author. Email: delale@itu.edu.tr
§Email: schnerr@flm.mw.tu-muenchen.de

well as in diesel injection nozzles. The first model of bubbly liquid flow through a converging–diverging nozzle was proposed by Tangren *et al.* (1949) using a barotropic relation. The problem was reconsidered by Ishii *et al.* (1993) by taking into account unsteady effects, but still neglecting bubble dynamics. A summary of barotropic models can be found in the book by Brennen (1995). For cavitating flows, it is essential to consider bubble dynamics together with the equations of nozzle flow. A continuum bubbly mixture flow model that couples spherical bubble dynamics, as described by the classical Rayleigh–Plesset equation, to the flow equations was proposed by van Wijngaarden (1968). Steady-state solutions of bubbly cavitating flows through converging–diverging nozzles have been investigated by Wang & Brennen (1998) and Delale *et al.* (2001) using the continuum bubbly liquid flow model. Assuming that the gas pressure inside the bubble obeys the polytropic law and lumping all damping mechanisms, in a crude manner, by a single damping coefficient in the form of viscous dissipation, both investigations have demonstrated bifurcation of steady-state solutions to flashing flow instabilities by varying the inlet void fraction (or inlet bubble radius or inlet cavitation number). A numerical investigation of unsteady bubbly cavitating flows in converging–diverging nozzles based on the same model has been carried out by Preston *et al.* (2002). They show that the instabilities encountered in the steady-state solutions of quasi-1D bubbly nozzle flows may correspond to unsteady bubbly shock waves formed in the diverging section of the nozzle and propagated downstream.

The aim of this investigation is to present a detailed analysis of quasi-1D unsteady bubbly cavitating flows in converging–diverging nozzles with the inclusion of bubble/bubble interactions as discussed in Delale *et al.* (2001). The description is, therefore, restricted solely to the investigation of the interplay between the overall compressibility of the continuum bubbly mixture and the flow unsteadiness using a damping coefficient which lumps all damping mechanisms, in a crude manner, in the form of viscous dissipation. From these model equations, the evolution equations for the flow speed and bubble radius are derived. The local pressure field, in this model, then follows exactly by its relation to the bubble radius, flow speed and its partial derivatives, showing explicitly the contributions arising from area change, two-phase mixture compressibility and flow unsteadiness.

The evolution equations obtained are then applied to the stability of steady-state quasi-1D bubbly cavitating nozzle flow solutions. Although the stability of both inviscid and viscous bubbly parallel flows have been investigated by d'Agostino *et al.* (1997) and d'Agostino & Burzagli (2000), it is important to investigate the temporal stability of cavitating nozzle flows in the quasi-1D approximation to find out whether such steady solutions are stable with respect to temporal perturbations. For the range of nozzle inlet conditions, where steady-state solutions exist, the temporal stability is examined by perturbing the two evolution equations for the flow speed and bubble radius using the corresponding steady-state solutions as base fields. A coupled system of linear partial differential equations (PDEs) is obtained for the temporal stability of the steady-state solutions. In particular, a normal mode analysis is carried out in the inlet region and stability diagrams are obtained by varying the cavitation number or inlet void fraction against the perturbation wave number k. Results show that steady-state solutions of the model equations are temporally stable only for very small wave numbers. The effect of damping mechanisms on the stability of the steady-state solutions seems to be negligible in the inlet region because of the very small growth rate of the bubbles. However, the stable regions of the stability diagram are seen to be broadened when the wall shear stress is taken into account.

2. Model equations for bubbly cavitating flows

We consider an unsteady quasi-1D cavitating nozzle flow and we assume that the initial distributions, inlet conditions and nozzle geometry are such that cavitation can occur in the nozzle. We use a slightly

modified version of the continuum bubbly mixture model, introduced by van Wijngaarden (1968) and later employed by Wang & Brennen (1998), Delale *et al.* (2001) and Preston *et al.* (2002), that couples the unsteady nozzle flow equations to spherical bubble dynamics. In this model, the effect of the relative motion between the bubbles and the surrounding liquid is neglected using a homogeneous two-phase flow model for the bubbly mixture. This effect may become important in certain cases and should then be taken into account (Noordzij & van Wijngaarden, 1974; Bieshuevel & van Wijngaarden, 1984; Zhang & Prosperetti, 1994; Wang & Chen, 2002). Keeping this in mind, the conventional continuity and momentum nozzle flow equations for the bubbly mixture can be written as

$$A' \frac{\partial \rho'}{\partial t'} + \frac{\partial}{\partial x'}(\rho' u' A') = 0, \tag{2.1}$$

$$\rho' \frac{\mathrm{d}u'}{\mathrm{d}t'} = -\frac{\partial p'}{\partial x'} - \frac{P'}{A'}\tau'_{\mathrm{w}}, \tag{2.2}$$

together with

$$\rho' = \rho'_{\ell}(1-\beta). \tag{2.3}$$

In (2.1–2.3), ρ' is the mixture density (given by (2.3) where the contribution from the dispersed gaseous phase has been neglected and where the liquid phase is assumed to be incompressible with constant density ρ'_{ℓ}), β is the void fraction, u' is the flow speed, p' is the mixture pressure and τ'_{w} is the wall shear stress, all presumably being functions of the axial coordinate x' (with origin at the throat) and the time t'. Moreover, A' is the nozzle cross-sectional area and P' is the wetted cross-sectional perimeter. It is also worthwhile to note that, in the momentum equation (2.2), the gravity effect is neglected and $\mathrm{d}/\mathrm{d}t' = \partial/\partial t' + u'\partial/\partial x'$ denotes the material or total derivative. The system of equations (2.1–2.3) is coupled to bubble dynamics through the void fraction β. For a cloud of monodispersed spherical bubbles of radius R', the void fraction β is defined by

$$\beta = \frac{4}{3}\pi R'^3 n', \tag{2.4}$$

where n' is the bubble population density per unit volume of the mixture. If creation (nucleation and bubble fission) and coagulation of bubbles are neglected, the bubble population density n' can be related to the void fraction β by

$$n' = \eta'_0(1-\beta), \tag{2.5}$$

where η'_0 is the number density of bubbles per unit volume of the liquid and is constant throughout the flow. It then follows from (2.4) and (2.5) that

$$\frac{R'^3(1-\beta)}{\beta} = \frac{3}{4\pi\eta'_0} = \text{constant} \tag{2.6}$$

throughout the flow. The system of equations (2.1–2.3) together with (2.6) is completed by a model equation for spherical bubble dynamics. It is well known that various damping mechanisms including viscous dissipation, liquid compressibility and thermal conduction through the gas/vapour bubble contribute to bubble dynamics (Nigmatulin *et al.*, 1981; Prosperetti & Lezzi, 1986; Prosperetti *et al.*, 1988; Prosperetti, 1991). In this investigation, the various damping mechanisms are lumped together, in an

ad hoc manner, in the form of viscous dissipation by an overall damping coefficient. Although the detailed structure of the damping mechanisms can not be treated by such a crude model, it is useful in providing information on the magnitude of the overall damping, relative to viscous damping. In particular, liquid compressibility and thermal damping dominate during violent collapse of cavitation bubbles. Deformation of bubbles near boundaries (Blake & Gibson, 1987), shape instabilities (Brenner *et al.*, 1995) and bubble fission (Brennen, 2002) also contribute significantly to energy losses within the bubble that has to be taken into account separately (Delale & Tunç, 2004). In this case, bubble collapse is non-spherical, and results using spherical bubble dynamics has to be interpreted statistically for a cloud of bubbles by a mean radius related to the volume of the bubbles. Moreover, inside such a cloud of bubbles, bubble/bubble interactions can become important. A model for spherical bubble dynamics which accounts for bubble/bubble interactions by a slightly modified local homogeneous mean field theory of Kubota *et al.* (1992) and for the various damping mechanisms by lumping them together, in an *ad hoc* manner, in the form of viscous dissipation with an overall damping coefficient has been employed by Delale *et al.* (2001) to study the bifurcation structure of steady-state cavitating nozzle flows. Here, we use this model for spherical bubble dynamics, which provides a modified Rayleigh–Plesset equation for the mean radius as

$$\frac{p'_{\mathrm{v}}-p'}{\rho'_{\ell}}=\frac{[1+(2/3)\pi\,\eta'_0(3\Lambda^2-1)R'^3]}{[1+(4/3)\pi\,\eta'_0R'^3]}R'\frac{\mathrm{d}^2R'}{\mathrm{d}t'^2}$$
$$+\frac{3}{2}\frac{[1+(8/3)\pi\,\eta'_0(2\Lambda^2-1)R'^3+(16/9)\pi^2\eta'^2_0\Lambda^2R'^6]}{[1+(4/3)\pi\,\eta'_0R'^3]^2}\left(\frac{\mathrm{d}R'}{\mathrm{d}t'}\right)^2$$
$$+\frac{2S'}{\rho'_{\ell}R'}+\frac{4\mu'_{\mathrm{eff}}}{\rho'_{\ell}R'}\frac{\mathrm{d}R'}{\mathrm{d}t'}-p'_{\mathrm{gi}}\left(\frac{R'_0}{R'}\right)^{3k}. \tag{2.7}$$

In (2.7), S' is the surface tension coefficient, p'_{v} is the partial vapour pressure inside the bubble, p'_{gi} is the initial gas pressure of the bubble at the inlet of the nozzle, k is the polytropic index (in particular, $k=1$ for isothermal expansion and $k=\gamma$ for isentropic expansion of the gas, where γ is the isentropic exponent of the gas), μ'_{eff} is the overall damping coefficient and Λ is the bubble/bubble interaction parameter defined by

$$\Lambda=\frac{\Delta r'}{R'} \tag{2.8}$$

with $\Delta r'$ denoting the range of interactions from the center of any fixed bubble (Kubota *et al.*, 1992; Delale *et al.*, 2001). We now normalize the mixture density, the gas and mixture pressures and the flow speed as

$$\rho=\frac{\rho'}{\rho'_{\ell}}=1-\beta,\quad p=\frac{p'}{p'_{\mathrm{i}}},\quad p_{\mathrm{v}}=\frac{p'_{\mathrm{v}}}{p'_{\mathrm{i}}},\quad p_{\mathrm{g}}=\frac{p'_{\mathrm{g}}}{p'_{\mathrm{i}}},\quad u=\frac{u'}{\sqrt{p'_{\mathrm{i}}/\rho'_{\ell}}}, \tag{2.9}$$

based on the liquid density ρ'_{ℓ}, the initial pressure at the nozzle inlet p'_{i} and a characteristic speed $\sqrt{p'_{\mathrm{i}}/\rho'_{\ell}}$. We also normalize the axial coordinate x' by a characteristic macroscale length H'_{i} (chosen as the nozzle inlet height), the cross-section area A' by the nozzle inlet area A'_{i}, the time coordinate t' by the characteristic flow time $\Theta'=H'_{\mathrm{i}}/\sqrt{p'_{\mathrm{i}}/\rho'_{\ell}}$ and the bubble radius R' by a characteristic

microscale length R'_{i} (chosen as the initial radius of bubbles, assumed to be monodispersed, at the inlet height) as

$$x = \frac{x'}{H'_{\mathrm{i}}}, \quad A = \frac{A'}{A'_{\mathrm{i}}}, \quad t = \frac{t'}{\Theta'} = \frac{\sqrt{p'_{\mathrm{i}}/\rho'_{\ell}}\,t'}{H'_{\mathrm{i}}} \quad \text{and} \quad R = \frac{R'}{R'_{\mathrm{i}}}. \tag{2.10}$$

Equations (2.1–2.7) then take the normalized form

$$\rho = 1 - \beta, \tag{2.11}$$

$$A\frac{\partial \rho}{\partial t} + \frac{\partial}{\partial x}(\rho u A) = 0, \tag{2.12}$$

$$\rho \frac{\mathrm{d}u}{\mathrm{d}t} = -\frac{\partial p}{\partial x} - C_{\mathrm{w}}\varphi\rho u^2, \tag{2.13}$$

$$R^3\left(\frac{1-\beta}{\beta}\right) = \frac{1-\beta_{\mathrm{i}}}{\beta_{\mathrm{i}}} = \kappa_{\mathrm{i}}^3, \tag{2.14}$$

$$\begin{aligned}\frac{p_{\mathrm{v}} - p}{L^2} = {} & \frac{[1 + (3\Lambda^2 - 1)(R/\kappa_{\mathrm{i}})^3/2]}{[1 + (R/\kappa_{\mathrm{i}})^3]} R\frac{\mathrm{d}^2 R}{\mathrm{d}t^2} \\ & + \frac{3}{2}\frac{[1 + 2(2\Lambda^2 - 1)(R/\kappa_{\mathrm{i}})^3 + \Lambda^2(R/\kappa_{\mathrm{i}})^6]}{[1 + (R/\kappa_{\mathrm{i}})^3]^2}\left(\frac{\mathrm{d}R}{\mathrm{d}t}\right)^2 \\ & + \frac{S_0}{L^2 R} + \frac{4}{L^2(\mathrm{Re})R}\frac{\mathrm{d}R}{\mathrm{d}t} - \frac{p_{\mathrm{gi}}}{L^2 R^{3k}}.\end{aligned} \tag{2.15}$$

where L is the ratio of micro scale to macro scale defined by

$$L = \frac{R'_{\mathrm{i}}}{H'_{\mathrm{i}}}, \tag{2.16}$$

C_{w} is the wall friction coefficient, φ is defined by

$$\varphi = \frac{H'_{\mathrm{i}} P'}{2A'}, \tag{2.17}$$

κ_{i} is a parameter defined in terms of the initial inlet void fraction β_{i} by

$$\kappa_{\mathrm{i}}^3 = \frac{1-\beta_{\mathrm{i}}}{\beta_{\mathrm{i}}}, \tag{2.18}$$

S_0 is the non-dimensional surface tension coefficient defined by

$$S_0 = \frac{2S'}{p'_{\mathrm{i}} R'_{\mathrm{i}}} \tag{2.19}$$

and Re is a typical Reynolds number, based on the overall damping coefficient μ'_{eff}, and is defined by

$$\mathrm{Re} = \frac{\rho'_{\ell} H'_{\mathrm{i}} \sqrt{p'_{\mathrm{i}}/\rho'_{\ell}}}{\mu'_{\mathrm{eff}}}. \tag{2.20}$$

Equations (2.11–2.15) constitute the model equations for unsteady cavitating nozzle flows with unknowns p, ρ, β, u and R and given area variation $A = A(x)$.

3. Evolution equations for the flow speed and bubble radius

By eliminating the void fraction β and the mixture density ρ between (2.11), (2.12) and (2.14), we obtain that

$$\frac{\mathrm{d}R}{\mathrm{d}t} - \frac{R}{3\beta(1-\beta)}\frac{\mathrm{d}\beta}{\mathrm{d}t} = \frac{\mathrm{d}R}{\mathrm{d}t} - \frac{R}{3\beta A}\frac{\partial}{\partial x}(uA) = 0. \tag{3.1}$$

We can further eliminate the pressure p between the momentum equation (2.13) and the modified Rayleigh–Plesset equation (2.15) by differentiating (2.15) with respect to x and by replacing the partial derivatives $\frac{\partial}{\partial x}\left(\frac{\mathrm{d}R}{\mathrm{d}t}\right)$ and $\frac{\partial}{\partial x}\left(\frac{\mathrm{d}^2R}{\mathrm{d}t^2}\right)$ from (3.1). After cumbersome manipulations, we arrive at the evolution equations for the bubble radius $R(x,t)$ and for the flow speed $u(x,t)$ as

$$\frac{\partial R}{\partial t} = -u\frac{\partial R}{\partial x} + \frac{1}{3R^2}(R^3 + \kappa_{\mathrm{i}}^3)\left[\left(\frac{1}{A}\frac{\mathrm{d}A}{\mathrm{d}x}\right)u + \frac{\partial u}{\partial x}\right] \tag{3.2}$$

and

$$\frac{\partial u}{\partial t} = a(x,t), \tag{3.3}$$

where the unsteady acceleration a satisfies the linear PDE

$$\frac{\partial^2 a}{\partial x^2} + g\frac{\partial a}{\partial x} + ha = s, \tag{3.4}$$

where the functions g and h are functions of R, $\partial R/\partial x$ and x, s is a function of R, u, $\partial R/\partial x$, $\partial u/\partial x$, $\partial^2 u/\partial x^2$, $\partial^3 u/\partial x^3$ and x, and they are defined by

$$g = \frac{F_1}{F_2}\frac{\partial R}{\partial x} + \frac{1}{A}\frac{\mathrm{d}A}{\mathrm{d}x}, \tag{3.5}$$

$$h = \frac{F_1}{F_2}\left(\frac{1}{A}\frac{\mathrm{d}A}{\mathrm{d}x}\right)\frac{\partial R}{\partial x} + \frac{F_3}{F_2} + \frac{\mathrm{d}}{\mathrm{d}x}\left(\frac{1}{A}\frac{\mathrm{d}A}{\mathrm{d}x}\right) \tag{3.6}$$

and

$$\begin{aligned} s = -\Bigg\{ & u\frac{\partial^3 u}{\partial x^3} + \left[\frac{F_1}{F_2}u\frac{\partial R}{\partial x} + \frac{F_4}{F_2}\frac{\partial u}{\partial x} + \frac{F_4}{F_2}u\left(\frac{1}{A}\frac{\mathrm{d}A}{\mathrm{d}x}\right) + \frac{F_5}{F_2}\right]\frac{\partial^2 u}{\partial x^2} \\ & + \frac{F_6}{F_2}\frac{\partial R}{\partial x}\left(\frac{\partial u}{\partial x}\right)^2 + \left[\frac{F_7}{F_2}u\left(\frac{1}{A}\frac{\mathrm{d}A}{\mathrm{d}x}\right) - 3\frac{F_3F_5}{RF_2}\right]\frac{\partial R}{\partial x}\frac{\partial u}{\partial x} + \frac{F_4}{F_2}\left(\frac{1}{A}\frac{\mathrm{d}A}{\mathrm{d}x}\right)\left(\frac{\partial u}{\partial x}\right)^2 \\ & + \left[\frac{F_8}{F_2}u\frac{\mathrm{d}}{\mathrm{d}x}\left(\frac{1}{A}\frac{\mathrm{d}A}{\mathrm{d}x}\right) + \frac{F_9}{F_2}u\left(\frac{1}{A}\frac{\mathrm{d}A}{\mathrm{d}x}\right)^2 + \frac{F_5}{F_2}\left(\frac{1}{A}\frac{\mathrm{d}A}{\mathrm{d}x}\right) + \frac{F_3}{F_2}u\right]\frac{\partial u}{\partial x} \end{aligned}$$

$$+\left[\frac{F_6}{F_2}u^2\left(\frac{1}{A}\frac{\mathrm{d}A}{\mathrm{d}x}\right)^2-3\frac{F_3F_5}{RF_2}u\left(\frac{1}{A}\frac{\mathrm{d}A}{\mathrm{d}x}\right)+\frac{F_1}{F_2}u^2\frac{\mathrm{d}}{\mathrm{d}x}\left(\frac{1}{A}\frac{\mathrm{d}A}{\mathrm{d}x}\right)+\frac{F_{10}}{F_2}\right]\frac{\partial R}{\partial x}$$

$$+\frac{F_9}{F_2}u^2\left(\frac{1}{A}\frac{\mathrm{d}A}{\mathrm{d}x}\right)\frac{\mathrm{d}}{\mathrm{d}x}\left(\frac{1}{A}\frac{\mathrm{d}A}{\mathrm{d}x}\right)+u^2\frac{\mathrm{d}^2}{\mathrm{d}x^2}\left(\frac{1}{A}\frac{\mathrm{d}A}{\mathrm{d}x}\right)$$

$$+\frac{F_5}{F_2}u\frac{\mathrm{d}}{\mathrm{d}x}\left(\frac{1}{A}\frac{\mathrm{d}A}{\mathrm{d}x}\right)+\frac{\partial p_\mathrm{v}/\partial x+\kappa_\mathrm{i}^3C_\mathrm{w}\varphi u^2/(R^3+\kappa_\mathrm{i}^3)}{F_2}\Bigg\}. \tag{3.7}$$

The functions F_j, $j = 1, 2, ..., 10$, entering (3.5–3.7), depend only on R and are given in Appendix A. The evolution equations (3.2) and (3.3) together with (3.4) can then be solved for a given nozzle configuration together with specified inlet and outlet boundary conditions for initially specified bubble radius and flow speed distributions. The solution for the rest of the hydrodynamic variables can then be related to this solution. In particular, the pressure field is given by

$$p=p_\mathrm{v}-\frac{L^2\kappa_\mathrm{i}^6}{18R^4}[(6\Lambda^2-1)(R/\kappa_\mathrm{i})^6+(6\Lambda^2-2)(R/\kappa_\mathrm{i})^3-1]\left[\left(\frac{1}{A}\frac{\mathrm{d}A}{\mathrm{d}x}\right)u+\frac{\partial u}{\partial x}\right]^2$$

$$-\frac{L^2\kappa_\mathrm{i}^3}{6R}[2+(3\Lambda^2-1)(R/\kappa_\mathrm{i})^3]\left[\frac{\partial a}{\partial x}+\left(\frac{1}{A}\frac{\mathrm{d}A}{\mathrm{d}x}\right)a+u\frac{\partial^2u}{\partial x^2}+\left(\frac{1}{A}\frac{\mathrm{d}A}{\mathrm{d}x}\right)u\frac{\partial u}{\partial x}+u^2\frac{\mathrm{d}}{\mathrm{d}x}\left(\frac{1}{A}\frac{\mathrm{d}A}{\mathrm{d}x}\right)\right]$$

$$-\frac{S_0}{R}+\frac{p_\mathrm{gi}}{R^{3k}}-\frac{4\kappa_\mathrm{i}^3}{3(\mathrm{Re})R^3}[1+(R/\kappa_\mathrm{i})^3]\left[\left(\frac{1}{A}\frac{\mathrm{d}A}{\mathrm{d}x}\right)u+\frac{\partial u}{\partial x}\right]. \tag{3.8}$$

Equation (3.8) expresses the explicit dependence of the pressure field on the bubble radius R, on the flow compressibility and its spatial derivative, the temporal acceleration a and its spatial derivative a_x, showing clearly how the local pressure field is affected by the two-phase mixture compressibility and flow unsteadiness. The last term that appears on the right-hand side of (3.8) is the contribution to the local pressure arising from the various damping effects (all lumped together, in an *ad hoc* manner, in the form of viscous dissipation) of spherical bubble dynamics. Finally, the void fraction β and the mixture density ρ follow from the formulas

$$\beta=1-\rho=\frac{R^3}{R^3+\kappa_\mathrm{i}^3}. \tag{3.9}$$

4. Temporal stability of steady-state quasi-1D bubbly cavitating nozzle flows

In this section, we utilize the above evolution equations to study the temporal stability of quasi-1D bubbly cavitating nozzle flow solutions of the van Wijngaarden (1968). It has been shown by Wang & Brennen (1998) and by Delale *et al.* (2001) that such steady-state solutions exist only for a certain range of a particular parameter when the rest of the inlet conditions are kept fixed for a given nozzle geometry. This parameter is usually chosen as the initial inlet void fraction β_i or the initial inlet cavitation number σ_i, defined by

$$\sigma_\mathrm{i}=\frac{p_\mathrm{i}'-p_\mathrm{v}'}{(1/2)\rho_\ell'^2u_{\mathrm{i}0}'^2}=\frac{1-p_\mathrm{v}}{(1/2)u_{\mathrm{i}0}^2}, \tag{4.1}$$

where u'_{i0} and u_{i0}, respectively, denote the dimensional and normalized initial flow speeds at the nozzle inlet. We herein study the temporal stability of these steady-state solutions for the range of parameters they exist. For this reason, we perturb the steady-state quasi-1D bubbly cavitating flow solutions of the normalized flow speed $\bar{u}(x)$ and the normalized bubble radius $\bar{R}(x)$ in the form

$$u = \bar{u}(x)[1 + \epsilon w(x,t)], \tag{4.2}$$

$$R = \bar{R}(x)[1 + \epsilon \phi(x,t)], \tag{4.3}$$

where ϵ is a small parameter, assumed to be much less than unity in magnitude ($\epsilon \ll 1$), and the time-dependent flow speed and the bubble radius perturbation functions, respectively, denoted by $w(x,t)$ and $\phi(x,t)$ are assumed to be of O(1) in magnitude (linear stability). Substitution of the perturbed field given by (4.2) and (4.3) into the evolution equations (3.2–3.4) yields to O(1) the steady-state quasi-1D bubbly cavitating nozzle flow equations for the flow speed $\bar{u}(x)$ and the bubble radius $\bar{R}(x)$. These equations can be shown to be equivalent to the third-order differential equation obtained by Delale *et al.* (2001) for the steady-state flow speed $\bar{u}(x)$. The linear PDEs for the perturbations $w(x,t)$ and $\phi(x,t)$, after cumbersome manipulations, then follow as

$$A_1\frac{\partial^3 w}{\partial x^3} + A_2\frac{\partial^3 w}{\partial x^2 \partial t} + A_3\frac{\partial^2 w}{\partial x^2} + A_4\frac{\partial^2 w}{\partial x \partial t} + A_5\frac{\partial w}{\partial x} + A_6\frac{\partial w}{\partial t} + A_7\frac{\partial \phi}{\partial x} + A_8 w + A_9\phi = 0 \tag{4.4}$$

and

$$C_1\frac{\partial^3 w}{\partial x^3} + C_2\frac{\partial^3 w}{\partial x^2 \partial t} + C_3\frac{\partial^2 w}{\partial x^2} + C_4\frac{\partial^2 w}{\partial x \partial t} + C_5\frac{\partial w}{\partial x} + C_6\frac{\partial w}{\partial t} + C_7 w + C_8\phi - \frac{\partial \phi}{\partial t} = 0, \tag{4.5}$$

where the coefficients $A_i, i = 1, 2, ..., 9$, are all the functions of $\bar{u}(x)$, $\bar{R}(x)$, the nozzle area $A(x)$ and its derivatives and are given in Appendix C. The coefficients $C_i, i = 1, 2, ..., 8$, entering (4.5) are defined as

$$C_1 = \bar{u}\frac{A_1}{A_7}, \quad C_2 = \bar{u}\frac{A_2}{A_7}, \quad C_3 = \bar{u}\frac{A_3}{A_7}, \quad C_4 = \bar{u}\frac{A_4}{A_7}, \quad C_5 = \bar{u}\frac{A_5}{A_7} + \frac{\bar{u}^2 A}{3(\bar{u}A - \lambda_i)}, \tag{4.6}$$

$$C_6 = \bar{u}\frac{A_6}{A_7}, \quad C_7 = \bar{u}\frac{A_8}{A_7} \quad \text{and} \quad C_8 = \bar{u}\frac{A_9}{A_7} - \frac{\lambda_i}{(\bar{u}A - \lambda_i)}\left[\frac{d\bar{u}}{dx} + \left(\frac{1}{A}\frac{dA}{dx}\right)\bar{u}\right] \tag{4.7}$$

with $\lambda_i = (1 - \beta_i)\bar{u}_i$, where β_i denotes the inlet void fraction and $\bar{u}_i$ is the normalized inlet flow speed in steady flow.

5. Normal mode analysis in the inlet region

The coefficients $A_i, i = 1, .., 9$, and $C_i, i = 1, .., 8$, entering (4.4) and (4.5) are all functions of the steady-state flow speed and the radius distributions $\bar{u}(x)$ and $\bar{R}(x)$ and of the nozzle area and its derivatives. The perturbations $w(x,t)$ and $\phi(x,t)$, on the other hand, enter the equations up to first order in the time derivative. Therefore, one can in principle cast the system into an eigenvalue problem using the transformation

$$w(x,t) = \tilde{w}(x)e^{st} \quad \text{and} \quad \phi(x,t) = \tilde{\phi}(x)e^{st} \tag{5.1}$$

to arrive at the generalized eigenvalue problem

$$L_1\psi = sL_2\psi \tag{5.2}$$

with

$$\psi = \begin{pmatrix} \tilde{\omega}(x) \\ \tilde{\phi}(x) \end{pmatrix}, \tag{5.3}$$

$$L_1 = \begin{pmatrix} A_1\dfrac{\partial^3}{\partial x^3} + A_3\dfrac{\partial^2}{\partial x^2} + A_5\dfrac{\partial}{\partial x} + A_8 & A_7\dfrac{\partial}{\partial x} + A_9 \\ C_1\dfrac{\partial^3}{\partial x^3} + C_3\dfrac{\partial^2}{\partial x^2} + C_5\dfrac{\partial}{\partial x} + C_7 & C_8 \end{pmatrix} \tag{5.4}$$

and

$$L_2 = \begin{pmatrix} -A_2\dfrac{\partial^2}{\partial x^2} - A_4\dfrac{\partial}{\partial x} - A_6 & 0 \\ -C_2\dfrac{\partial^2}{\partial x^2} - C_4\dfrac{\partial}{\partial x} - C_6 & 1 \end{pmatrix}. \tag{5.5}$$

Temporal stability then demands that the real parts s_{R} of the eigenvalues s are negative ($s_{\mathrm{R}} < 0$) provided that the eigenvalues s are obtained by the solution of the eigenvalue problem given by (5.2). The generalized eigenvalue problem can, in principle, be solved by discretization or using spectral methods. Even if the complete spectrum of the generalized eigenvalue problem is obtained, it would be difficult to establish a physical criterion to sort out the physically relevant eigenvalues from the rest. Thus, the numerical solution in this case does not seem to be feasible, despite the difficulties in obtaining the complete spectrum. Fortunately, in regions where all the coefficients A_i, $i = 1, .., 9$, and C_i, $i = 1, .., 8$, entering (4.4) and (4.5) remain constants, the temporal stability problem can be solved exactly by normal mode analysis. In quasi-1D bubbly cavitating nozzle flows, we find these coefficients to be almost constant in the nozzle inlet region where variations in both flow and area variations are relatively small. Thus, we can carry a normal mode analysis of the temporal stability of the steady-state solutions in the nozzle inlet region. For this reason, we let

$$w(x,t) = \hat{w}\,\mathrm{e}^{\mathrm{i}(kx-\omega t)} \quad \text{and} \quad \phi(x,t) = \hat{\phi}\,\mathrm{e}^{\mathrm{i}(kx-\omega t)}) \tag{5.6}$$

in the inlet region of the nozzle, where k denotes the wave number, ω denotes the angular frequency, $\hat{w}$ and $\hat{\phi}$, respectively, denote the amplitudes of the flow speed and the radius (both much less than unity in magnitude) and where all the coefficients entering the linear PDE system given by (4.4) and (4.5) are nearly constants. Substitution of (5.6) into (4.4) and (4.5) leads to the dispersion relation

$$L\omega^2 + M\omega + N = 0, \tag{5.7}$$

where the complex coefficients L, M and N are given by

$$L = L_{\mathrm{R}} + \mathrm{i}L_{\mathrm{I}} = (A_6 - A_2k^2) + \mathrm{i}A_4k, \tag{5.8}$$

$$M = M_{\mathrm{R}} + \mathrm{i}M_{\mathrm{I}}$$

$$= [(A_4C_8 - A_5 - A_9C_4 - A_7C_6)k + (A_1 + A_7C_2)k^3]$$
$$+ \mathrm{i}[(A_8 - A_6C_8 + A_9C_6) + (A_2C_8 - A_3 - A_7C_4 - A_9C_2)k], \tag{5.9}$$

$$N = N_\mathrm{R} + \mathrm{i}N_\mathrm{I}$$
$$= [(A_8C_8 - A_9C_7) + (A_7C_5 + A_9C_3 - A_3C_8)k^2 - A_7C_1k^4]$$
$$+ \mathrm{i}[(A_5C_8 - A_7C_7 - A_9C_5)k + (A_7C_3 + A_9C_1 - A_1C_8)k^3] \tag{5.10}$$

with subscripts R and I denoting the real and imaginary parts of complex numbers. For temporal stability, the wave number k is real and given. The angular frequency ω, on the other hand, is complex ($\omega = \omega_\mathrm{R} + \mathrm{i}\omega_\mathrm{I}$). Therefore, for temporal stability, the imaginary part ω_I of the angular frequency must be negative ($\omega_\mathrm{I} < 0$). From the dispersion relation (5.7), we obtain the fourth-degree polynomial equation

$$\varepsilon_4\omega_\mathrm{I}^4 + \varepsilon_3\omega_\mathrm{I}^3 + \varepsilon_2\omega_\mathrm{I}^2 + \varepsilon_1\omega_\mathrm{I} + \varepsilon_0 = 0 \tag{5.11}$$

for ω_I, where the coefficients ε_i, $i = 0, \ldots, 4$, are all polynomials in the wave number k and are given in Appendix D. To investigate the sign of ω_I given by (5.11) for a given wave number k, we first note that all the coefficients ε_i, $i = 0, \ldots, 4$, are even functions of the wave number k. Therefore, one only needs to investigate the sign of ω_I for $k > 0$. Setting $\varepsilon_0 = 0$, which results in a polynomial of degree 5 in k^2, we find those real positive roots k_i, $i \leqslant 5$, for which ω_I vanishes. From the sign of $-\varepsilon_1/\varepsilon_4$, we determine the sign of ω_I in the immediate vicinity of each k_i, $i \leqslant 5$. We then identify those regions where $\omega_\mathrm{I} < 0$ as the stable regions of quasi-1D steady-state cavitating nozzle flows.

6. Results and discussion

We now consider a two-phase bubbly flow with bubbles containing water vapour and air in water at an isothermal temperature of 20°C, implying a constant partial vapour pressure $p'_\mathrm{v} = 0.0234$ bar, a constant surface tension coefficient $S' = 7.1 \times 10^{-2}$ N/m and a constant water viscosity $\mu'_\ell = 10^{-3}$ kg/ms. The inlet pressure is set at the fixed value $p'_\mathrm{i} = 1.013$ bar. The nozzle geometry employed by Preston *et al.* (2002), as shown in Figs 1 and 2, and whose area in our normalization is given by

$$A(x) = 1 - 0.25\exp\left[-\left(\frac{x - 150L}{30L}\right)^2\right] \tag{6.1}$$

is considered. Furthermore, for a quasi-1D nozzle, we have $\varphi = 1/A$. The wall friction coefficient is evaluated for a smooth wall using the turbulent correlation

$$\frac{1}{C_\mathrm{w}^{1/2}} = 1.768\ln[(\mathrm{Re}_f)C_\mathrm{w}^{1/2}] - 0.94 \tag{6.2}$$

which was verified experimentally (for details see Ward-Smith, 1980) where the Reynolds number Re_f is related to Re of (2.20) by

$$\mathrm{Re}_f = 2uA(\mathrm{Re})\frac{\mu'_\mathrm{eff}}{\mu'_\ell}. \tag{6.3}$$

The inlet bubble radius is fixed at $R'_{\mathrm{i}0} = 40$ μm together with $L = 8 \times 10^{-4}$. Here, we neglect bubble/bubble interactions so that $\Lambda = 1$ since they are not important in the inlet region. We set the inlet

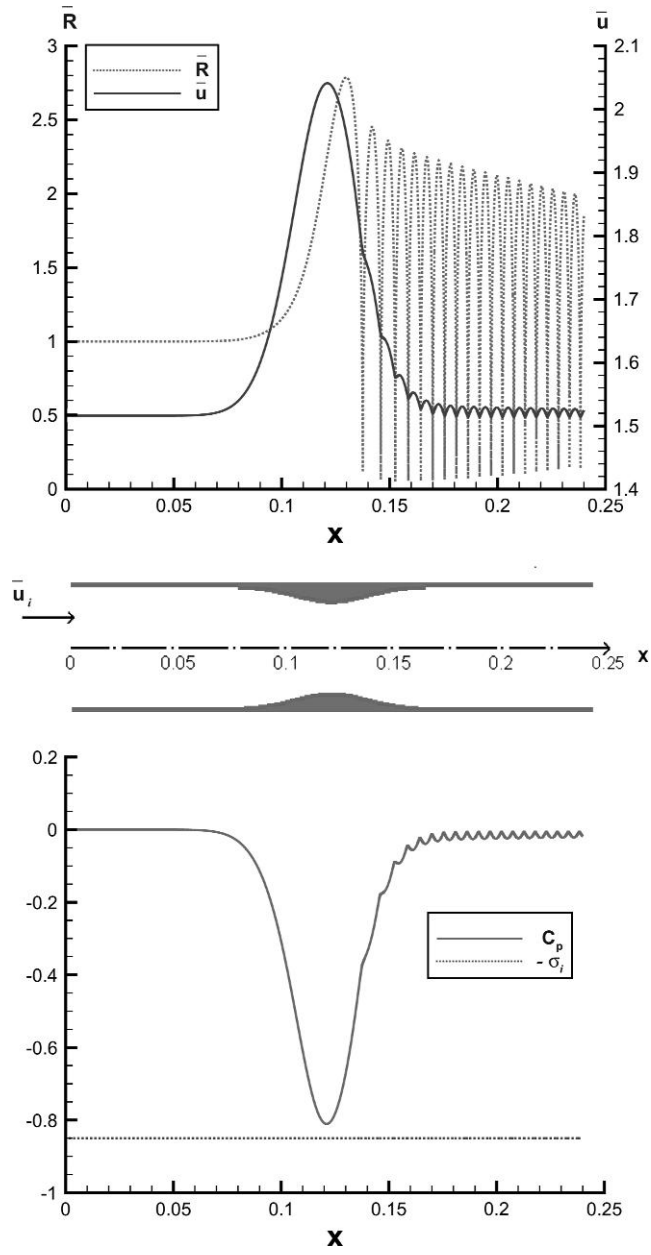

FIG. 1. The steady-state non-cavitating bubble radius, flow speed (top figure) and pressure coefficient (bottom figure) distributions of water with air bubbles along the axial coordinate of the nozzle employed by Preston *et al.* (2002) (middle figure) with damping coefficient $\mu'_{\text{eff}}/\mu'_{\ell} = 1.0$, bubble/bubble interaction parameter $\Lambda = 1.0$, inlet bubble radius $R'_{\text{i}} = 40$ μm , micro to macro length ratio $L = 8 \times 10^{-4}$, inlet pressure $p'_{\text{i}} = 1.013$ bar, inlet void fraction $\beta_{\text{i}} = 10^{-3}$ and cavitation number $\sigma_{\text{i}} = 0.85$.

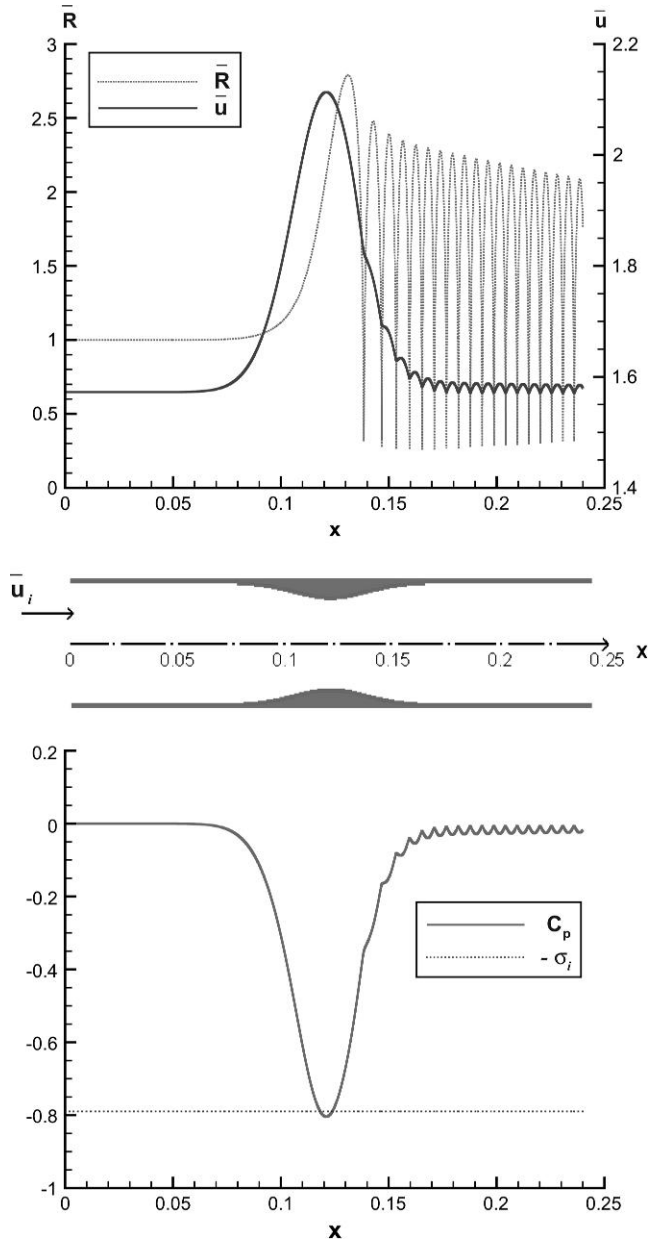

FIG. 2. The steady-state cavitating bubble radius, flow speed (top figure) and pressure coefficient (bottom figure) distributions of water with air bubbles along the axial coordinate of the nozzle employed by Preston *et al.* (2002) (middle figure) with damping coefficient $\mu'_{\rm eff}/\mu'_{\ell} = 1.0$, bubble/bubble interaction parameter $\Lambda = 1.0$, inlet bubble radius $R'_{\rm i} = 40$ μm , micro to macro length ratio $L = 8 \times 10^{-4}$, inlet pressure $p'_{\rm i} = 1.013$ bar, inlet void fraction $\beta_{\rm i} = 10^{-3}$ and cavitation number $\sigma_{\rm i} = 0.79$.

void fraction at the value $\beta_i = 10^{-3}$ and vary the cavitation number σ in the range between 0.7 and 1.0 for both the inviscid ($C_w = 0$) and the turbulent flow case where the friction coefficient C_w is given by (6.2). All damping mechanisms of bubble dynamics are taken into account by a single damping coefficient μ'_{eff}/μ'_ℓ in the form of viscous dissipation (in particular, $\mu'_{eff}/\mu'_\ell = 1$ corresponds to the case where all damping mechanisms, except viscous dissipation, are neglected). It is well known from the work of Wang & Brennen (1998) and Delale *et al.* (2001) that steady-state solutions under specified conditions exist only if the cavitation number σ_i is above some critical value σ_{ic}. It follows that under the above stated conditions, $\sigma_{ic} = 0.78$ when $\mu'_{eff}/\mu'_\ell = 1$ and $\sigma_{ic} = 0.72$ when $\mu'_{eff}/\mu'_\ell = 30$ for both the inviscid case and the case where turbulent wall shear stress is taken into account. Typical steady-state solutions of the flow speed $\bar{u}(x)$, the bubble radius $\bar{R}(x)$ and the pressure coefficient $C_p(x)$ are shown in Figs 1 and 2 for non-cavitating ($\sigma_i > -(C_p)_{min}$) and cavitating ($\sigma_i < -(C_p)_{min}$) bubbly flows, respectively, where $(C_p)_{min}$ denotes the minimum of the pressure coefficient (the effect of the turbulent wall shear stress is negligible in this case). These results are in good agreement with the steady-state solutions obtained by Preston *et al.* (2002). When a normal mode analysis to the steady-state base field solutions is applied in the inlet region, as described above, from the sign of ω_I, we find the temporally stable ones corresponding to real wave numbers k and construct the stability diagrams. Figure 3 shows such a stability diagram for the variation of the cavitation number σ_i against the perturbation wave number k under the conditions stated above. As has been demonstrated by Wang & Brennen (1998) and Delale *et al.* (2001), we note that there are no steady-state solutions below a critical cavitation number under the specified conditions and nozzle geometry. As the steady-state solutions obtained above a critical cavitation number are perturbed with respect to flow unsteadiness (temporal stability), we find that stable solutions exist only for very small wave numbers of the perturbations (in fact, there exist stable regions for very large wave

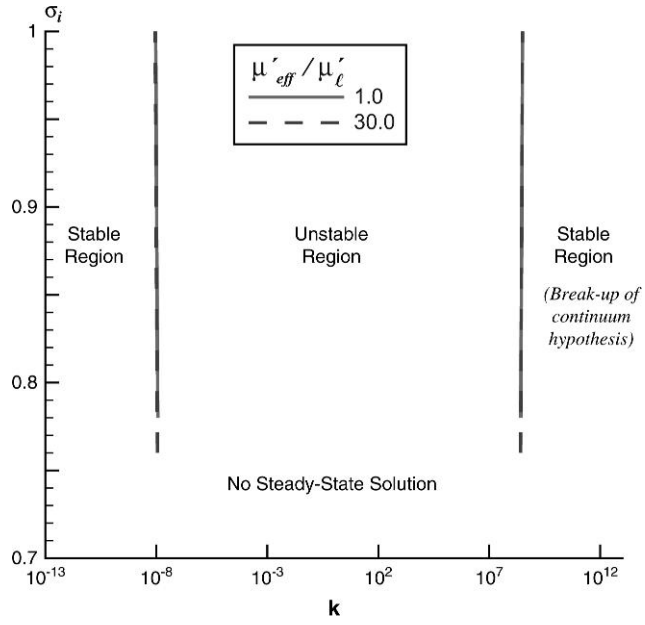

FIG. 3. Stability diagram showing the variation of the cavitation number σ, varied between 0.7 and 1.0, versus the perturbation wave number k for different values of the damping coefficient μ'_{eff}/μ'_ℓ in the inviscid case of quasi-1D bubbly (cavitating/non-cavitating) nozzle flows, keeping the rest of the conditions specified in Fig. 1 fixed.

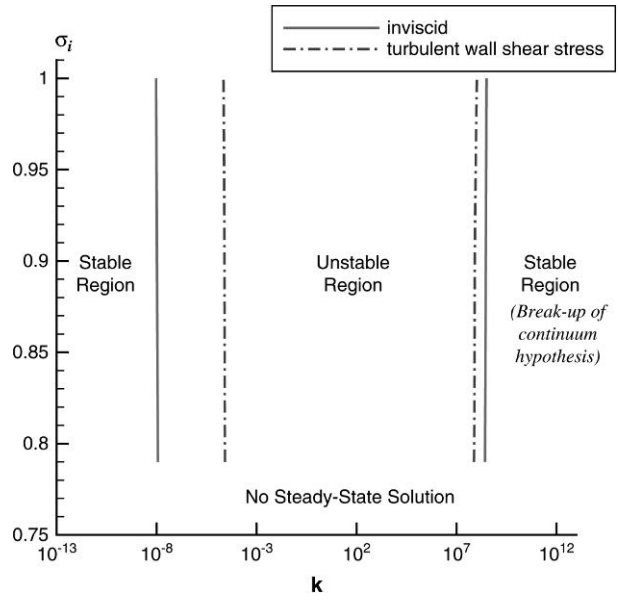

FIG. 4. Stability diagram showing the variation of the cavitation number σ_i, varied between 0.75 and 1.0, versus the perturbation wave number k for the inviscid and turbulent wall shear stress cases in quasi-1D bubbly (cavitating/non-cavitating) nozzle flows, keeping the rest of the conditions specified in Fig. 1 fixed.

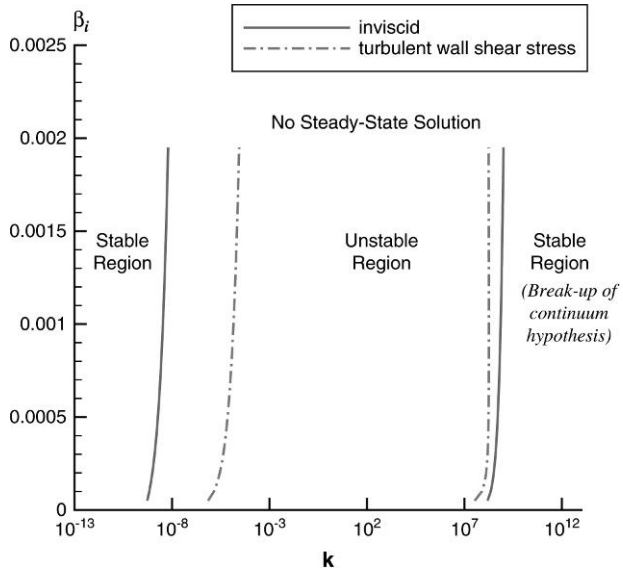

FIG. 5. Stability diagram showing the variation of the inlet void fraction β_i, varied between 10^{-5} and 10^{-3}, versus the perturbation wave number k for the inviscid and turbulent wall shear stress cases in quasi-1D bubbly cavitating nozzle flows, keeping the rest of the conditions specified in Fig. 2 fixed.

numbers of the perturbations as well; however, these steady-state solutions are to be discarded on physical grounds as they correspond to limits where the continuum hypothesis breaks down). As the damping coefficient $\mu'_{\text{eff}}/\mu'_{\ell}$ is increased, we observe no significant change of the stable region in the stability diagram since the bubble growth rate in the inlet region is relatively small. However, when the effect of the turbulent wall shear stress is taken into account, the stability region shown in Fig. 4 is broadened as expected. We should note that the effect of turbulence in this case is only considered for the steady-state turbulent wall shear stress and turbulent fluctuations are not taken into account. We also can construct stability diagrams at a fixed cavitation number σ_{i} by varying the inlet void fraction β_{i} in some range where steady-state solutions can be observed. Figure 5 shows such a stability diagram of the steady-state solutions when the cavitation number is fixed at $\sigma_{\text{i}} = 0.79$ while the void fraction β_{i} is varied in the range 10^{-5}–10^{-3}. In this case, no steady-state solutions exist above the critical value $\beta_{\text{c}} = 2 \times 10^{-3}$. Once again, physically stable steady-state solutions are observed for very small wave numbers and the stability region is seen to be broadened when the effect of the turbulent wall shear stress is taken into account.

7. Conclusions

In this investigation, we have considered model equations for quasi-1D bubbly cavitating nozzle flows and their application to the temporal stability of the corresponding steady-state solutions. The model equations benefit the classical unsteady nozzle flow equations for a bubbly mixture in the homogeneous two-phase flow model. These equations are supplemented by a modified Rayleigh–Plesset equation that takes bubble/bubble interactions into account in the mean field theory. All damping mechanisms, in an *ad hoc* manner, are lumped together in the form of viscous dissipation by a single damping coefficient and a polytropic law for the growth and collapse of the bubbles is assumed. The complete system of equations is then uncoupled leading to two evolution equations, one for the flow speed and the other for the bubble radius. For the range of nozzle inlet conditions, where steady-state solutions exist, the temporal stability is examined by perturbing the two evolution equations for the flow speed and bubble radius using the corresponding steady-state solutions as base fields. A coupled system of linear PDEs is obtained for the temporal stability of the steady-state solutions. In particular, a normal mode analysis is carried out in the inlet region and stability diagrams are obtained by varying the cavitation number or inlet void fraction against the perturbation wave number k. Results show that steady-state solutions of the model equations are temporally stable only for very small wave numbers. The stable regions of the stability diagram for the inlet region of the nozzle are seen to be broadened by the effect of turbulent wall shear stress.

This investigation has enlightened the difficulty in achieving real steady-state cavitating bubbly flows, even in the inlet region of the nozzle. Real cavitating flows are spatially multidimensional; therefore, the model equations have to be considered in two or three dimensions. For real cavitating nozzle flows, the model equations should also be supplemented by a realistic thermal damping model by considering the energy equation for each phase replacing the polytropic law, especially in regions of bubble collapse. These issues are beyond the present work and will be considered in future investigations.

Acknowledgement

Part of this work was completed in partial fulfilment of the Ph.D. thesis of Ms Şenay Pasinlioğlu at Istanbul Technical University.

Funding

The Scientific and Technological Research Council of Turkey (105M035 to C.F.D.); Istanbul Technical University Research Foundation Scientific Research Projects (31532 to Ş.P.)

References

BIESHUEVEL, A. & VAN WIJNGAARDEN, L. (1984) Two-phase flow equations for a dilute dispersion of gas bubbles in liquids. *J. Fluid Mech.*, **148**, 301–318.

BLAKE, J. R. & GIBSON, D. C. (1987) Cavitation bubbles near boundaries. *Ann. Rev. Fluid Mech.*, **19**, 99–123.

BRENNEN, C. E. (1995) *Cavitation and Bubble Dynamics*. Oxford: Oxford University Press.

BRENNEN, C. E. (2002) Fission of collapsing cavitating bubbles. *J. Fluid Mech.*, **472**, 153–166.

BRENNER, M. P., LOHSE, D. & DUPONT, T. F. (1995) Bubble shape oscillations and the onset of sonoluminescence. *Phys. Rev. Lett.*, **75**, 954–957.

D'AGOSTINO, L. & BURZAGLI, F. (2000) On the stability of parallel bubbly cavitating flows. *ASME J. Fluids Eng.*, **122**, 471–480.

D'AGOSTINO, L., D'AURIA, F. & BRENNEN, C. E. (1997) On the inviscid stability of parallel bubbly flows. *J. Fluid Mech.*, **339**, 261–274.

DELALE, C. F., SCHNERR, G. H. & SAUER, J. (2001) Quasi-one-dimensional steady-state cavitating nozzle flows. *J. Fluid Mech.*, **427**, 167–204.

DELALE, C. F. & TUNÇ, M. (2004) A bubble fission model for collapsing cavitation bubbles. *Phys. Fluids*, **16**, 4200–4203.

ISHII, R., UMEDA, Y., MURATA, S. & SHISHIDO, N. (1993) Bubbly flows through a converging-diverging nozzle. *Phys. Fluids*, **A5**, 1630–1643.

KUBOTA, A., KATO, H. & YAMAGUCHI, H. (1992) A numerical study of unsteady cavitation on a hydraulic section. *J. Fluid Mech.*, **240**, 59–96.

NIGMATULIN, R. I., KHABEEV, N. S. & NAGIEV, F. B. (1981) Dynamics, heat and mass transfer of vapor-gas bubbles in a liquid. *Int. J. Heat Mass Transf.*, **24**, 1033–1044.

NOORDZIJ, L. & VAN WIJNGAARDEN, L. (1974) Relaxation effects, caused by relative motion, on shock waves in gas-bubble/liquid mixtures. *J. Fluid Mech.*, **66**, 115–143.

PRESTON, A., COLONIUS, T. & BRENNEN, C. E. (2002) A numerical investigation of unsteady bubbly cavitating nozzle flows. *Phys. Fluids*, **14**, 300–311.

PROSPERETTI, A. (1991) The thermal behaviour of oscillating gas bubbles. *J. Fluid Mech.*, **222**, 587–616.

PROSPERETTI, A., CRUM, L. A. & COMMANDER, K. W. (1988) Nonlinear bubble dynamics. *J. Acoust. Soc. Am.*, **83**, 502–514.

PROSPERETTI, A. & LEZZI, A. (1986) Bubble dynamics in compressible liquid. Part 1. First-order theory. *J. Fluid Mech.*, **168**, 457–478.

TANGREN, R. F., DODGE, C. H. & SEIFERT, H. S. (1949) Compressibility effects in two-phase flow. *J. Appl. Phys.*, **20**, 637–645.

VAN WIJNGAARDEN, L. (1968) On the equations of motion for mixtures of liquid and gas bubbles. *J. Fluid Mech.*, **33**, 465–474.

WANG, Y. C. & BRENNEN, C. E. (1998) One-dimensional bubbly cavitating flows through a converging-diverging nozzle. *ASME J. Fluids Eng.*, **120**, 166–170.

WANG, Y. C. & CHEN, E. (2002) Effects of phase relative motion on critical bubbly flows through a converging-diverging nozzle. *Phys. Fluids*, **14**, 3215–3223.

WARD-SMITH, A. J. (1980) *Internal Fluid Flow*. Oxford: Clarendon Press, p.186.

ZHANG, D. Z. & PROSPERETTI, A. (1994) Ensemble phase-averaged equations for bubbly flows. *Phys. Fluids*, **6**, 2956–2970.

Appendix A

The functions F_j, $j = 1, 2, \ldots, 10$, entering (3.5–3.7) are defined as

$$F_1(\zeta) = -\frac{L^2\kappa_\mathrm{i}}{3\zeta^2[1+\zeta^3]}[(3\Lambda^2-1)\zeta^6 + (3\Lambda^2-2)\zeta^3 - 1], \tag{A.1}$$

$$F_2(\zeta) = -\frac{L^2\kappa_\mathrm{i}^2}{6\zeta}[2 + (3\Lambda^2-1)\zeta^3], \tag{A.2}$$

$$F_3(\zeta) = \frac{1}{[1+\zeta^3]}, \tag{A.3}$$

$$F_4(\zeta) = -\frac{L^2\kappa_\mathrm{i}^2}{18\zeta^4}[(21\Lambda^2-5)\zeta^6 + (12\Lambda^2+2)\zeta^3 - 2], \tag{A.4}$$

$$F_5(\zeta) = -\frac{4}{3(\mathrm{Re})\zeta^3}[1+\zeta^3], \tag{A.5}$$

$$F_6(\zeta) = -\frac{L^2\kappa_\mathrm{i}}{18\zeta^5(1+\zeta^3)}[(12\Lambda^2-2)\zeta^9 + 6\Lambda^2\zeta^6 - 6(\Lambda^2-1)\zeta^3 + 4], \tag{A.6}$$

$$F_7(\zeta) = -\frac{L^2\kappa_\mathrm{i}}{9\zeta^5(1+\zeta^3)}[(21\Lambda^2-5)\zeta^9 + (15\Lambda^2-6)\zeta^6 + (-6\Lambda^2+3)\zeta^3 + 4], \tag{A.7}$$

$$F_8(\zeta) = -\frac{L^2\kappa_\mathrm{i}^2}{18\zeta^4}[(39\Lambda^2-11)\zeta^6 + (12\Lambda^2+14)\zeta^3 - 2], \tag{A.8}$$

$$F_9(\zeta) = -\frac{L^2\kappa_\mathrm{i}^2}{18\zeta^4}[(12\Lambda^2-2)\zeta^6 + (12\Lambda^2-4)\zeta^3 - 2], \tag{A.9}$$

$$F_{10}(\zeta) = \frac{S_0}{{\kappa_\mathrm{i}}^2\zeta^2} - \frac{3k\,p_{\mathrm{gi}}}{{\kappa_\mathrm{i}}^{3k+1}\zeta^{3k+1}}, \tag{A.10}$$

where ζ is defined by

$$\zeta = \zeta(x,t) = \frac{R(x,t)}{\kappa_\mathrm{i}}. \tag{A.11}$$

Appendix B

The functions f_j, $j = 1, 2, \ldots, 10$, entering (C.8) and (C.9) are defined as

$$f_1(\bar{\zeta}) = \frac{L^2\kappa_\mathrm{i}}{3(\bar{\zeta})^2[1+(\bar{\zeta})^3]^2}[(3\Lambda^2-1)(\bar{\zeta})^9 + 6\Lambda^2(\bar{\zeta})^6 + (3\Lambda^2+3)(\bar{\zeta})^3 + 2] \tag{B.1}$$

$$f_2(\bar{\zeta}) = \frac{L^2\kappa_\mathrm{i}^2}{3\bar{\zeta}}[(3\Lambda^2-1)(\bar{\zeta})^3 - 1] \tag{B.2}$$

$$f_3(\bar{\zeta}) = \frac{3\bar{\zeta}^3}{[1+(\bar{\zeta})^3]^2} \tag{B.3}$$

$$f_4(\bar{\zeta}) = \frac{L^2\kappa_{\mathrm{i}}^2}{9(\bar{\zeta})^4}[(21\Lambda^2-5)(\bar{\zeta})^6 - (6\Lambda^2+1)(\bar{\zeta})^3 + 4] \tag{B.4}$$

$$f_5(\bar{R}) = -\frac{4}{(\mathrm{Re})(\bar{\zeta})^3} \tag{B.5}$$

$$f_6(\bar{\zeta}) = \frac{L^2\kappa_{\mathrm{i}}}{18(\bar{\zeta})^5[1+(\bar{\zeta})^3]^2}[(12\Lambda^2-2)(\bar{\zeta})^{12} + (36\Lambda^2-8)(\bar{\zeta})^9 + (36\Lambda^2-30)(\bar{\zeta})^6 + (12\Lambda^2-44)(\bar{\zeta})^3 - 20] \tag{B.6}$$

$$f_7(\bar{\zeta}) = \frac{L^2\kappa_{\mathrm{i}}}{9(\bar{\zeta})^5[1+(\bar{\zeta})^3]^2}[(21\Lambda^2-5)(\bar{\zeta})^{12} + (54\Lambda^2-8)(\bar{\zeta})^9 + (45\Lambda^2-21)(\bar{\zeta})^6 + (12\Lambda^2-38)(\bar{\zeta})^3 - 20] \tag{B.7}$$

$$f_8(\bar{\zeta}) = \frac{L^2\kappa_{\mathrm{i}}^2}{18(\bar{\zeta})^4}[(78\Lambda^2-22)(\bar{\zeta})^6 - (12\Lambda^2+14)(\bar{\zeta})^3 + 8] \tag{B.8}$$

$$f_9(\bar{\zeta}) = \frac{L^2\kappa_{\mathrm{i}}^2}{18(\bar{\zeta})^4}[(24\Lambda^2-4)(\bar{\zeta})^6 - (12\Lambda^2-4)(\bar{\zeta})^3 + 8] \tag{B.9}$$

$$f_{10}(\bar{\zeta}) = \frac{2S_0}{{\kappa_{\mathrm{i}}}^2(\bar{\zeta})^2} - \frac{3k(3k+1)p_{\mathrm{gi}}}{{\kappa_{\mathrm{i}}}^{3k+1}(\bar{\zeta})^{3k+1}}, \tag{B.10}$$

where $\bar{\zeta}$ is defined by

$$\bar{\zeta} = \frac{\bar{R}(x)}{\kappa_{\mathrm{i}}}. \tag{B.11}$$

Appendix C

The functions A_j, $j = 1, 2, \ldots, 9$, entering (4.4) and (4.5) are

$$A_1 = F_2\bar{u}^2, \tag{C.1}$$

$$A_2 = F_2\bar{u}, \tag{C.2}$$

$$A_3 = 3F_2\bar{u}\frac{\mathrm{d}\bar{u}}{\mathrm{d}x} + \left\{F_1\bar{u}\frac{\mathrm{d}\bar{R}}{\mathrm{d}x} + F_4\left[\frac{\mathrm{d}\bar{u}}{\mathrm{d}x} + \left(\frac{1}{A}\frac{\mathrm{d}A}{\mathrm{d}x}\right)\bar{u}\right] + F_5\right\}\bar{u}, \tag{C.3}$$

$$A_4 = 2F_2\frac{\mathrm{d}\bar{u}}{\mathrm{d}x} + \left[F_1\frac{\mathrm{d}\bar{R}}{\mathrm{d}x} + F_2\left(\frac{1}{A}\frac{\mathrm{d}A}{\mathrm{d}x}\right)\right]\bar{u}, \tag{C.4}$$

$$A_5 = [3F_2 + F_4]\bar{u}\frac{\mathrm{d}^2\bar{u}}{\mathrm{d}x^2} + 2F_4\left(\frac{\mathrm{d}\bar{u}}{\mathrm{d}x}\right)^2 + \left[(F_1 + F_6)\bar{u}\frac{\mathrm{d}\bar{R}}{\mathrm{d}x} + 2F_4\left(\frac{1}{A}\frac{\mathrm{d}A}{\mathrm{d}x}\right)\bar{u} + F_5\right]2\frac{\mathrm{d}\bar{u}}{\mathrm{d}x} + \left[F_7\left(\frac{1}{A}\frac{\mathrm{d}A}{\mathrm{d}x}\right)\bar{u} - \frac{3F_3F_5}{\bar{R}}\right]\frac{\mathrm{d}\bar{R}}{\mathrm{d}x}\bar{u} + \left\{F_8\bar{u}\frac{\mathrm{d}}{\mathrm{d}x}\left(\frac{1}{A}\frac{\mathrm{d}A}{\mathrm{d}x}\right) + F_9\left(\frac{1}{A}\frac{\mathrm{d}A}{\mathrm{d}x}\right)^2\bar{u} + F_5\left(\frac{1}{A}\frac{\mathrm{d}A}{\mathrm{d}x}\right) + F_3\bar{u}\right\}\bar{u}, \tag{C.5}$$

$$A_6 = F_2\frac{\mathrm{d}^2\bar{u}}{\mathrm{d}x^2} + \left[F_1\frac{\mathrm{d}\bar{R}}{\mathrm{d}x} + F_2\left(\frac{1}{A}\frac{\mathrm{d}A}{\mathrm{d}x}\right)\right]\frac{\mathrm{d}\bar{u}}{\mathrm{d}x} + \left[F_1\left(\frac{1}{A}\frac{\mathrm{d}A}{\mathrm{d}x}\right)\frac{\mathrm{d}\bar{R}}{\mathrm{d}x} + F_2\frac{\mathrm{d}}{\mathrm{d}x}\left(\frac{1}{A}\frac{\mathrm{d}A}{\mathrm{d}x}\right) + F_3\right]\bar{u}, \tag{C.6}$$

$$A_7 = F_1\bar{u}\bar{R}\frac{\mathrm{d}^2\bar{u}}{\mathrm{d}x^2} + F_6\bar{R}\left(\frac{\mathrm{d}\bar{u}}{\mathrm{d}x}\right)^2 + \left[F_7\bar{u}\left(\frac{1}{A}\frac{\mathrm{d}A}{\mathrm{d}x}\right) - \frac{3F_3F_5}{\bar{R}}\right]\bar{R}\frac{\mathrm{d}\bar{u}}{\mathrm{d}x} + \left[F_1\frac{\mathrm{d}}{\mathrm{d}x}\left(\frac{1}{A}\frac{\mathrm{d}A}{\mathrm{d}x}\right)\bar{u}^2 + F_6\left(\frac{1}{A}\frac{\mathrm{d}A}{\mathrm{d}x}\right)^2\bar{u}^2 - \frac{3F_3F_5}{\bar{R}}\left(\frac{1}{A}\frac{\mathrm{d}A}{\mathrm{d}x}\right)\bar{u} + F_{10}\right]\bar{R}, \tag{C.7}$$

$$A_8 = -F_5\frac{\mathrm{d}^2\bar{u}}{\mathrm{d}x^2} + \left[\frac{3F_3F_5}{\bar{R}}\frac{\mathrm{d}\bar{R}}{\mathrm{d}x} - F_5\left(\frac{1}{A}\frac{\mathrm{d}A}{\mathrm{d}x}\right)\right]\frac{\mathrm{d}\bar{u}}{\mathrm{d}x} + \left[\frac{3F_3F_5}{\bar{R}}\left(\frac{1}{A}\frac{\mathrm{d}A}{\mathrm{d}x}\right)\frac{\mathrm{d}\bar{R}}{\mathrm{d}x} - F_5\frac{\mathrm{d}}{\mathrm{d}x}\left(\frac{1}{A}\frac{\mathrm{d}A}{\mathrm{d}x}\right)\right]\bar{u} - 2F_{10}\frac{\mathrm{d}\bar{R}}{\mathrm{d}x} - 2\frac{\partial p_\mathrm{v}}{\partial x}, \tag{C.8}$$

$$A_9 = -f_2\bar{u}\frac{\mathrm{d}^3\bar{u}}{\mathrm{d}x^3} + \left\{(F_1 - f_1)\bar{u}\frac{\mathrm{d}\bar{R}}{\mathrm{d}x} - f_4\left[\frac{\mathrm{d}\bar{u}}{\mathrm{d}x} + \left(\frac{1}{A}\frac{\mathrm{d}A}{\mathrm{d}x}\right)\bar{u}\right] - f_5\right\}\frac{\mathrm{d}^2\bar{u}}{\mathrm{d}x^2} + \left[(F_6 - f_6)\frac{\mathrm{d}\bar{R}}{\mathrm{d}x} - f_4\left(\frac{1}{A}\frac{\mathrm{d}A}{\mathrm{d}x}\right)\right]\left(\frac{\mathrm{d}\bar{u}}{\mathrm{d}x}\right)^2 + \left[(F_7 - f_7)\left(\frac{1}{A}\frac{\mathrm{d}A}{\mathrm{d}x}\right)\bar{u} + \frac{3}{\bar{R}}[F_3f_5 + F_5f_3]\right]\frac{\mathrm{d}\bar{R}}{\mathrm{d}x}\frac{\mathrm{d}\bar{u}}{\mathrm{d}x} + \left[-f_8\frac{\mathrm{d}}{\mathrm{d}x}\left(\frac{1}{A}\frac{\mathrm{d}A}{\mathrm{d}x}\right)\bar{u} - f_9\left(\frac{1}{A}\frac{\mathrm{d}A}{\mathrm{d}x}\right)^2\bar{u} - f_5\left(\frac{1}{A}\frac{\mathrm{d}A}{\mathrm{d}x}\right) - f_3\bar{u}\right]\frac{\mathrm{d}\bar{u}}{\mathrm{d}x} + \left[(F_6 - f_6)\left(\frac{1}{A}\frac{\mathrm{d}A}{\mathrm{d}x}\right)^2\bar{u}^2 + (F_1 - f_1)\frac{\mathrm{d}}{\mathrm{d}x}\left(\frac{1}{A}\frac{\mathrm{d}A}{\mathrm{d}x}\right)\bar{u}^2 + \frac{3}{\bar{R}}[F_3f_5 + F_5f_3]\left(\frac{1}{A}\frac{\mathrm{d}A}{\mathrm{d}x}\right)\bar{u} + (F_{10} - f_{10})\right]\frac{\mathrm{d}\bar{R}}{\mathrm{d}x} - f_2\frac{\mathrm{d}^2}{\mathrm{d}x^2}\left(\frac{1}{A}\frac{\mathrm{d}A}{\mathrm{d}x}\right)\bar{u}^2 - f_9\left(\frac{1}{A}\frac{\mathrm{d}A}{\mathrm{d}x}\right)\frac{\mathrm{d}}{\mathrm{d}x}\left(\frac{1}{A}\frac{\mathrm{d}A}{\mathrm{d}x}\right)\bar{u}^2 - f_3\varphi C_\mathrm{w}\bar{u}^2 - f_5\frac{\mathrm{d}}{\mathrm{d}x}\left(\frac{1}{A}\frac{\mathrm{d}A}{\mathrm{d}x}\right)\bar{u}, \tag{C.9}$$

where the functions F_i, $i = 1, 2, \ldots, 10$, are all evaluated at $\zeta = \bar{\zeta} = \bar{R}(x)/\kappa_\mathrm{i}$.

Appendix D

The functions ε_j, $j = 0, 1, \ldots, 4$, entering (5.11) are

$$\varepsilon_0 = L_{\mathrm{R}}^2 L_{\mathrm{I}} N_{\mathrm{I}}^2 - 2L_{\mathrm{R}} L_{\mathrm{I}}^2 N_{\mathrm{R}} N_{\mathrm{I}} + L_{\mathrm{I}}^3 N_{\mathrm{R}}^2 + L_{\mathrm{R}} L_{\mathrm{I}} M_{\mathrm{I}}^2 N_{\mathrm{R}} - L_{\mathrm{R}} L_{\mathrm{I}} M_{\mathrm{R}} M_{\mathrm{I}} N_{\mathrm{I}} + L_{\mathrm{I}}^2 M_{\mathrm{R}}^2 N_{\mathrm{I}} - L_{\mathrm{I}}^2 M_{\mathrm{R}} M_{\mathrm{I}} N_{\mathrm{R}}, \tag{D.1}$$

$$\varepsilon_1 = 4L_{\mathrm{R}}^2 L_{\mathrm{I}} M_{\mathrm{I}} N_{\mathrm{R}} - 4L_{\mathrm{R}} L_{\mathrm{I}}^2 M_{\mathrm{R}} N_{\mathrm{R}} - 4L_{\mathrm{I}}^3 M_{\mathrm{R}} N_{\mathrm{I}} + 4L_{\mathrm{R}} L_{\mathrm{I}}^2 M_{\mathrm{I}} N_{\mathrm{I}} + L_{\mathrm{I}}^2 M_{\mathrm{R}} M_{\mathrm{I}}^2 - L_{\mathrm{R}} L_{\mathrm{I}} M_{\mathrm{R}}^2 M_{\mathrm{I}} + L_{\mathrm{I}}^2 M_{\mathrm{R}}^3 - L_{\mathrm{R}} L_{\mathrm{I}} M_{\mathrm{I}}^3, \tag{D.2}$$

$$\varepsilon_2 = 8L_{\mathrm{R}} L_{\mathrm{I}}^2 M_{\mathrm{R}} M_{\mathrm{I}} - 5L_{\mathrm{R}}^2 L_{\mathrm{I}} M_{\mathrm{I}}^2 + 4L_{\mathrm{R}}^3 L_{\mathrm{I}} N_{\mathrm{R}} + 4L_{\mathrm{I}}^4 N_{\mathrm{I}} - L_{\mathrm{I}}^3 M_{\mathrm{I}}^2 - L_{\mathrm{R}}^2 L_{\mathrm{I}} M_{\mathrm{R}}^2 + 4L_{\mathrm{R}} L_{\mathrm{I}}^3 N_{\mathrm{R}} + 4L_{\mathrm{R}}^2 L_{\mathrm{I}}^2 N_{\mathrm{I}} - 5L_{\mathrm{I}}^3 M_{\mathrm{R}}^2, \tag{D.3}$$

$$\varepsilon_3 = 8L_{\mathrm{I}}(L_{\mathrm{R}}^2 + L_{\mathrm{I}}^2)[L_{\mathrm{I}} M_{\mathrm{R}} - L_{\mathrm{R}} M_{\mathrm{I}}], \tag{D.4}$$

$$\varepsilon_4 = -4L_{\mathrm{I}}(L_{\mathrm{R}}^2 + L_{\mathrm{I}}^2)^2, \tag{D.5}$$

where L_{R}, L_{I}, M_{R}, M_{I}, N_{R} and N_{I} are given by (5.8–5.10).